ORGANIC PROCESS RESEARCH & DEVELOPMENT
OPR&D

Supporting information for

A Scalable Synthesis of (*R*,*R*)-*N*,*N*-Dibenzyl-2-fluorocyclohexan-1-amine with CsF under Hydrogen Bonding Phase-Transfer Catalysis

Anna Chiara Vicini,† Diké-Michel Alozie,‡[a] Philippe Courtes,‡[a] Giulia Roagna,† Catherine Aubert,‡[b] Victor Certal,‡[c] Youssef El-Ahmad,‡[c] Sébastien Roy,‡[b] Véronique Gouverneur†*

†University of Oxford, Chemistry Research Laboratory, 12 Mansfield Road, Oxford OX1 3TA, United Kingdom

‡Sanofi R&D, 13 Quai Jules Guesde, 94403 Vitry sur Seine Cedex, France

[a] *Process Safety*

[b] *IDD Isotope Chemistry*

[c] *Small Molecules Medicinal Chemistry*

*To whom correspondence should be addressed: veronique.gouverneur@chem.ox.ac.uk

Screening Reactions 2
CsF Particle Distribution 4
CsBr Particle Distribution and Morphology 5
Dynochem Calculations 8
DSC Reports 13
Reaction Calorimetry 16
Catalyst Recovery 17
NMR Spectra 21
HPLC Traces 24

Screening Reactions

Table S1: Solvent and Concentration Screening (Reaction with KF)

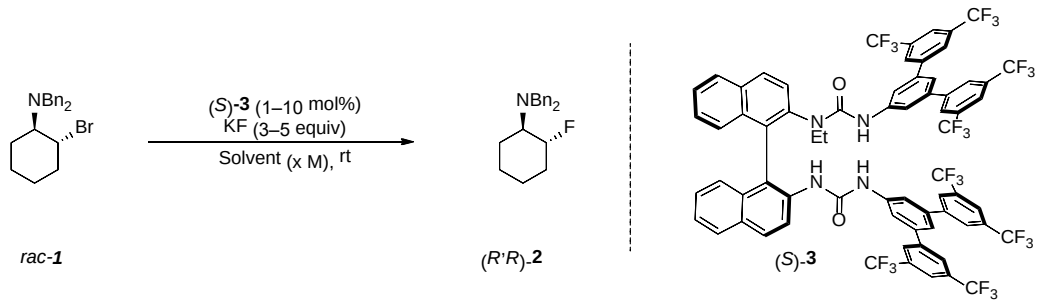

Entry	Solvent (Conc./M)	KF Equiv	(*S*)-3 Loading (mol%)	Time (h)	Yield[a]	e.r.[b]
1	$PhCF_3$ (0.5 M)	5	5	48	65%	84.5:15.5
2	$PhCF_3$ (0.5 M)	5	2	48	21%	–
3	$PhCF_3$ (0.5 M)	5	1	48	9%	–
4	$PhCF_3$ (0.5 M)	5	1	72	14%	–
5	$PhCF_3$ (1 M)	5	1	72	15%	–
6	$PhCF_3$ (2 M)	5	1	72	24%	–
7	$PhCF_3$ (2 M)	3	1	72	27%	84.5:15.5
8	1,2-difluorobenzene (2 M)	3	1	72	25%	81:19
9	CH_2Cl_2 (2 M)	3	1	72	45%	81:19
10	**$CHCl_3$ (2 M)**	3	1	72	**59%**	**81.5:18.5**

Conditions: *rac*-**1** (0.5 mmol), KF (3–5 equiv), (*S*)-**3** (1–10 mol%), rt, stirring at 900 rpm. [a] Yield determined by ^{19}F NMR using 4-fluoroanisole as internal standard. [b] e.r. determined by HPLC on a chiral non-racemic stationary phase.

Table S2: Additive Screening (Reaction with KF)

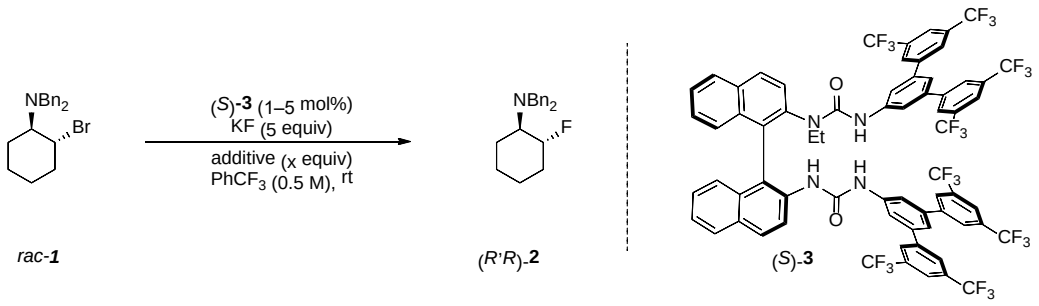

Entry	(*S*)-3 Loading	Additive (equiv)	Time (h)	Yield[a]	e.r.[b]
1	5 mol%	–	24	31%	85:15
2	"	18-crown-6 (0.5)	24	No reaction	–
3	"	TBABr (0.5)	24	No reaction	–
4	"	KI (0.5)	24	21% [c]	–
5	"	KOTf (0.5)	24	50%	85:15
6	1 mol%	–	48	9%	–
7	"	KOTf (0.1)	48	10%	–
8	"	KOTf (0.5)	48	traces	–

Conditions: *rac*-**1** (0.1 mmol), KF (5 equiv), (*S*)-**3** (1–5 mol%), $PhCF_3$ (0.5 M) rt, stirring at 900 rpm for 24 h (for 5 mol% catalyst loading) or 48 h (for 1 mol% catalyst loading). [a] Yield determined by ^{19}F NMR using 4-fluoroanisole as internal standard. [b] e.r. determined by HPLC on a chiral non-racemic stationary phase. [c] 61% of the corresponding iodide was detected: determined by ^{1}H NMR using 4-fluoroanisole as internal standard.

Table S3: Effect of CsF Equivalents, Catalyst Loading and Additives

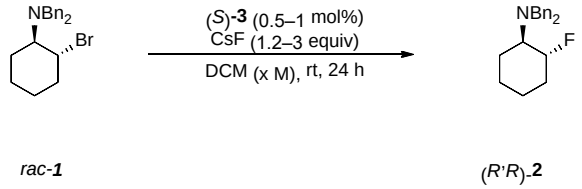

rac-***1*** (*R*'*R*)-**2**

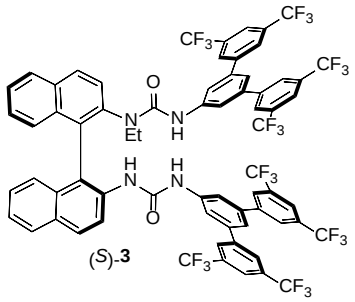

(*S*)-**3**

Entry	CsF Equiv	Additive (Equiv)	Concentration (M)	(*S*)-3 Loading (mol%)	Yield[a]	e.r. [b]
1	3	–	1	1	97%	82:18
2	3	–	1	0.5	88%	81:19
3	3	–	1	0.2	33%	79:21
4	1.2	–	1	0.5	42%	81.5:18.5
5	**1.2**	–	**2**	**0.5**	**87%**	**81:19**
6	1.2	KI (0.1)	1	0.5	43%[c]	82:18
7	1.2	KI (0.5)	1	0.5	40%[d]	81.5:18.5

Conditions: *rac*-**1** (0.5 mmol), CsF, (S)-**3**, rt, stirring in CH_2Cl_2 at 900 rpm for 24 h. [a] Yield determined by ^{19}F NMR using 4-fluoroanisole as internal standard. Isolated yields in parenthesis; [b] e.r. determined by HPLC on a chiral non-racemic stationary phase; [c] Traces of the corresponding iodide formed; [d] 17% of the corresponding iodide was detected; determined by ^{1}H NMR using 4-fluoroanisole as internal standard.

CsF Particle Distribution

Optical Microscopy (Transmission) Analysis

Sample preparation: few milligrams of CsF are placed on a glass slide and few drops of silicon oil 47V100 are added. To avoid breakage of the agglomerates, care has been taken to not exert any pressure when the coverslip was placed on top of the sample.

Result: The particle size is comprised between 2 µm and 300 µm. They appear as plates and irregular prisms.

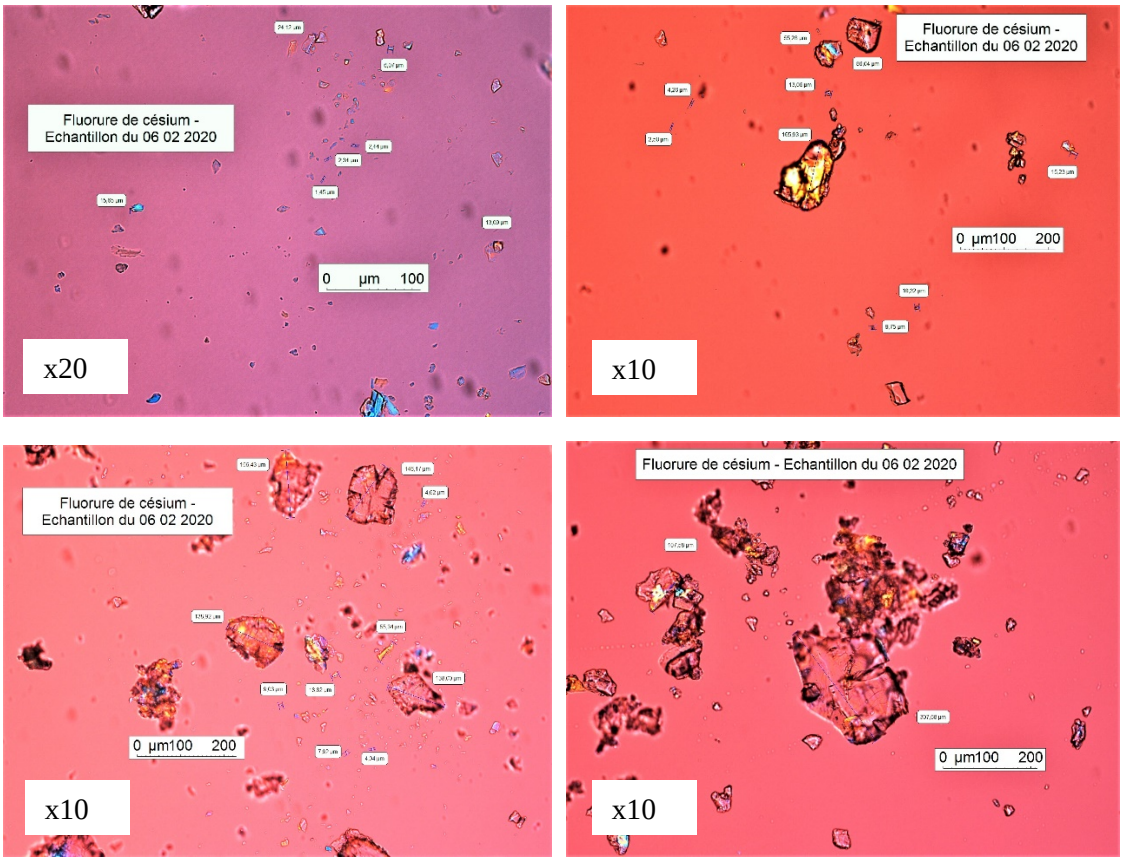

Figure S1: Analysis of CsF particles.

CsBr Particle Distribution and Morphology

Optical Microscopy (Transmission) Analysis

Sample preparation: The sample consist of large agglomerates. To observe the single particles, few milligrams of CsBr are placed on a glass slide and few drops of silicon oil 47V100 are added. Significant force was necessary to break some agglomerates to partially reveal the base particles. A coverslip on oil was used to protect this hygroscopic solid.

Result: Despite the pressure exert on the coverslip, some agglomerates are still visible. The single particles have mostly a spherical shape whose maximum size does not exceed 6 µm. The smallest particles are around 0.6 µm (detection limit for the x40 magnification).

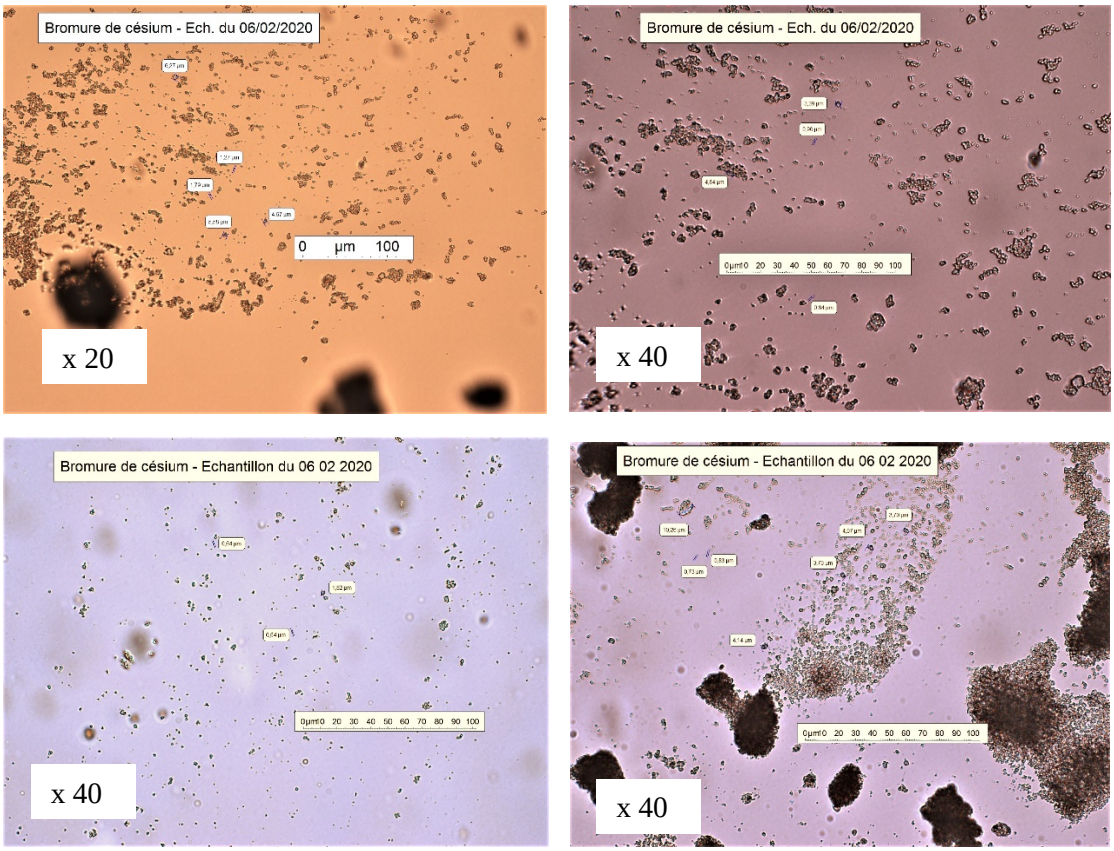

Figure S2: Optical microscopy analysis of CsBr particles formed in the 200 g scale fluorination of *rac*-**1** with CsF under HB-PTC.

SEM analysis

Coating: 120s.
Voltage: 10 kV–15 kV

Sample preparation: the sample was coated with gold for 120 s and pulverized on a sticky support to observe the single particles.

Result: The sample consist of agglomerates (~ 100 µm) of spherical particle. The size of the single particles is mostly comprised between 5–10 µm, with few being as small as 1 µm.

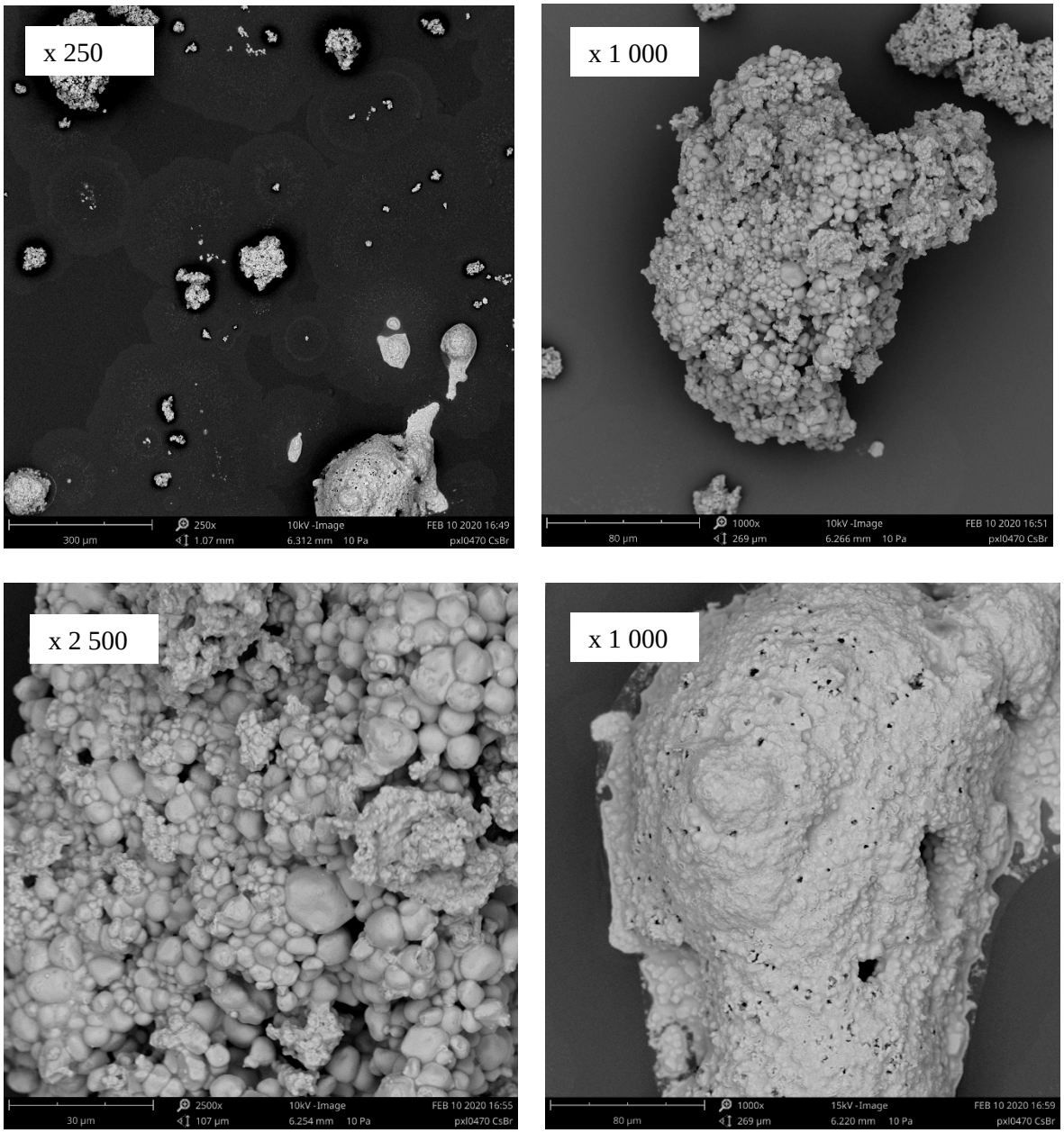

Figure S3: SEM analysis of CsBr particles formed in the 200 g scale fluorination of *rac*-**1** with CsF under HB-PTC. Agglomerates.

Small particles (1–2 µm)

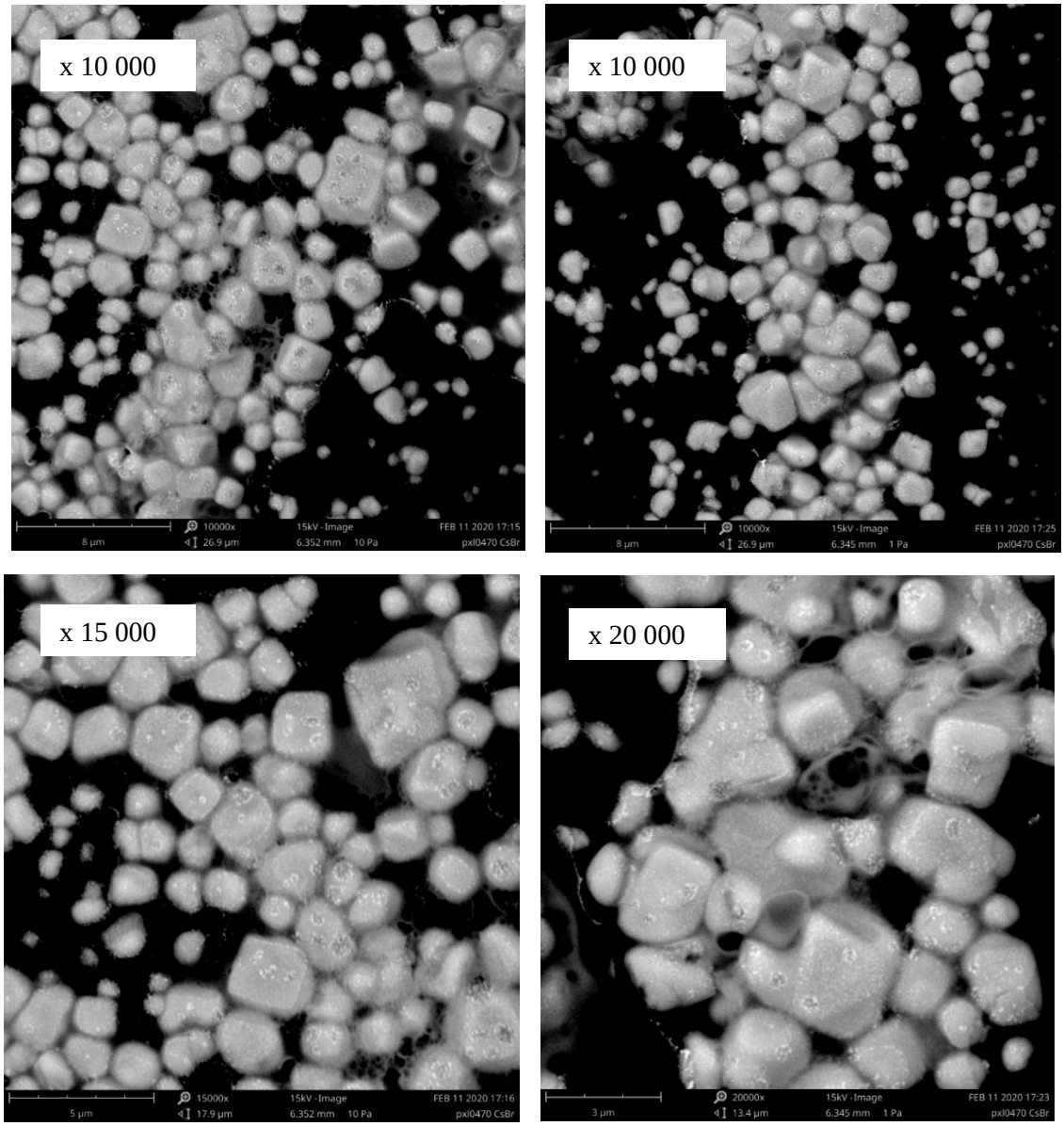

Figure S4: SEM analysis of CsBr particles formed in the 200 g scale fluorination of *rac*-**1** with CsF under HB-PTC. Small particles.

Dynochem Calculations

Physical Properties

Liquid density (ρ_L): 1756.55 kg/m^3
Liquid dynamic viscosity (μ_L): 0.57 Pa*s
Particle density (ρ_P): 4200 kg/m^3
Average density of slurry in kg/m^3: 1506 kg/m^3

Reactors Geometrical Parameters

	TOP45 (22 mL)	**OptiMax1001**	**Radleys 1 L-reactor**	**RC1 APO1 0.5 RTC 3w**
Base shape	Flat	Hemispherical	Hemispherical	Hemispherical
Inner diameter, T (mm)	20	101	100	70
Total height to tan (mm)	50	172	172	166
Maximum volume (L), *from database*	0.02	1.00	1.20	0.40
Base height (mm)	0.0	50.5	50.0	35.0
Base volume (L)	0.00	0.27	0.26	0.09
Impeller type	4-bladed flat blade turbine	4-bladed pitched blade turbine	4-bladed pitched blade turbine	4-bladed pitched blade turbine
Tip diameter (mm)	15.0	45.0	50.0	35.0
Clearance (mm)	5.0	10.0	20.0	10.0
Projected blade width (mm)	5.0	15.0	15.0	12.0
Impeller Power Number	3.2	1.8	1.7	1.0
Degree of baffling (%)	100% baffled	98% baffled	100% baffled	31% baffled

Suspension Characteristic

TOP45 (22 mL)

	Particle size (µm)	**100**	**200**
Mixing duty	Liquid volume (L)	0.0063	0.0063
	Mass of solids (kg)	0.00156	0.00156
	Total volume of solids & liquid (L)	0.0068	0.0068
	Mass ratio of solid to liquid (%)	0.02	0.02
	Total surface area (m^2)	20	20
	Agitator speed, N (rpm)	**0.00159**	**2050**
Performance at N	Correlation used	Zwietering	Zwietering
	Suspension condition	*Probably suspended*	*Probably suspended*
	Total power input, P (W)	0.15	0.15
	Power input per unit mass, ε (W/kg)	16.928	16.928
	Reynolds number, Re	$1.95*10^4$	$1.95*10^4$
	Vessel flow regime	Turbulent	Turbulent
	Tip speed, V_{tip} (m/s)	1.61	1.61
	Bulk liquid velocity (m/s)	0.21	0.21
	Torque per unit volume (N/m^2)	106.40	106.40
	Estimated maximum ε (trailing vortex) (W/kg)	***334.72***	***334.72***
	Vessel averaged turbulent shear rate (1/s)	6551	6551
	Impeller averaged turbulent shear rate (1/s)	***11138***	***11138***
	Impeller averaged laminar shear rate (1/s)	376	376
	Particle settling velocity (cm/s)	1.93	4.23
Performance at N_{JS}	**Just suspended speed, N_{JS} (rpm)**	**1929**	**2216**
	Total power input, P_{JS} (W)	0.12	0.18
	Power input per unit mass, ε_{JS} (W/kg)	14.106	21.380
	Reynolds number, Re_{JS} (-)	$1.83*10^4$	$2.11*10^4$
	Tip speed, V_{tip_JS} (m/s)	1.52	1.74
	Bulk liquid velocity (m/s)	0.20	0.23
	Vessel averaged shear rate (1/s)	5980	7363
	Impeller averaged shear rate (1/s)	10167	12518
	Impeller averaged laminar shear rate (1/s)	354	406

OptiMax1001

	Particle size (µm)	**200**
Mixing duty	Liquid volume (L)	0.43
	Mass of solids (kg)	0.10400
	Total volume of solids & liquid (L)	0.450
	Mass ratio of solid to liquid (%)	181
	Total surface area (m^2)	0.0222
	Agitator speed, N (rpm)	**1100**
Performance at N	Correlation used	Zwietering
	Suspension condition	*Solids suspended*
	Total power input, P (W)	3.16
	Power input per unit mass, ε (W/kg)	5.495
	Reynolds number, Re	$9.41* 10^4$
	Vessel flow regime	Turbulent
	Tip speed, V_{tip} (m/s)	2.59
	Bulk liquid velocity (m/s)	0.24
	Torque per unit volume (N/m^2)	64.37
	Estimated maximum ε (trailing vortex) (W/kg)	***307.90***
	Vessel averaged turbulent shear rate (1/s)	3733
	Impeller averaged turbulent shear rate (1/s)	***9972***
	Impeller averaged laminar shear rate (1/s)	202
	Particle settling velocity (cm/s)	4.23
Performance at N_{JS}	**Just suspended speed, N_{JS} (rpm)**	**795**
	Total power input, P_{JS} (W)	1.19
	Power input per unit mass, ε_{JS} (W/kg)	2.074
	Reynolds number, Re_{JS} (-)	$6.80* 10^4$
	Tip speed, V_{tip_JS} (m/s)	1.87
	Bulk liquid velocity (m/s)	0.17
	Vessel averaged shear rate (1/s)	2293
	Impeller averaged shear rate (1/s)	3733
	Impeller averaged laminar shear rate (1/s)	9972

Radleys 1 L-reactor

	Particle size (µm)	**12**	**100**	**200**
Mixing duty	Liquid volume (L)	0.43	0.43	0.43
	Mass of solids (kg)	0.10400	0.10400	0.10400
	Total volume of solids & liquid (L)	0.450	0.450	0.450
	Mass ratio of solid to liquid (%)	18.1	18.1	18.1
	Total surface area (m^2)	0.0223	0.0223	0.0223
	Agitator speed, N (rpm)	**678**	**678**	**678**
Performance at N	Correlation used	Zwietering	Zwietering	Zwietering
	Suspension condition	*Solids suspended*	*Solids suspended*	*Probably suspended*
	Total power input, P (W)	1.12	1.12	1.12
	Power input per unit mass, ε (W/kg)	1.953	1.953	1.953
	Reynolds number, Re	$7.16* 10^4$	$7.16* 10^4$	$7.16* 10^4$
	Vessel flow regime	Turbulent	Turbulent	Turbulent
	Tip speed, V_{tip} (m/s)	1.77	1.77	1.77
	Bulk liquid velocity (m/s)	0.20	0.20	0.20
	Torque per unit volume (N/m^2)	37.11	37.11	37.11
	Estimated maximum ε (trailing vortex) (W/kg)	***81.98***	***81.98***	***81.98***
	Vessel averaged turbulent shear rate (1/s)	2225	2225	2225
	Impeller averaged turbulent shear rate (1/s)	***5075***	***5075***	***5075***
	Impeller averaged laminar shear rate (1/s)	124	124	124
	Particle settling velocity (cm/s)	0.18	1.93	4.23
Performance at N_{JS}	**Just suspended speed, N_{JS} (rpm)**	**517**	**791**	**908**
	Total power input, P_{JS} (W)	0.50	1.78	2.70
	Power input per unit mass, ε_{JS} (W/kg)	0.868	3.096	4.693
	Reynolds number, Re_{JS} (-)	$5.47* 10^4$	$8.35* 10^4$	$9.59* 10^4$
	Tip speed, V_{tip_JS} (m/s)	1.35	2.07	2.38
	Bulk liquid velocity (m/s)	0.15	0.24	0.27
	Vessel averaged shear rate (1/s)	1483	2802	3449
	Impeller averaged shear rate (1/s)	3383	6391	7868
	Impeller averaged laminar shear rate (1/s)	95	145	166

RC1 APO1 0.5 RTC 3w

	Particle size (µm)	**12**	**100**	**200**
Mixing duty	Liquid volume (L)	0.21	0.21	0.21
	Mass of solids (kg)	0.05200	0.05200	0.05200
	Total volume of solids & liquid (L)	0.225	0.225	0.225
	Mass ratio of solid to liquid (%)	18.1	18.1	18.1
	Total surface area (m^2)	0.0154	0.0154	0.0154
	Agitator speed, N (rpm)	**600**	**600**	**600**
Performance at N	Correlation used	Zwietering	Zwietering	Zwietering
	Suspension condition	*Probably suspended*	*Not suspended*	*Not suspended*
	Total power input, P (W)	0.08	0.08	0.08
	Power input per unit mass, ε (W/kg)	0.269	0.269	0.269
	Reynolds number, Re	$3.11* 10^4$	$3.11* 10^4$	$3.11* 10^4$
	Vessel flow regime	*Turbulent*	*Turbulent*	*Turbulent*
	Tip speed, V_{tip} (m/s)	1.10	1.10	1.10
	Bulk liquid velocity (m/s)	0.10	0.10	0.10
	Torque per unit volume (N/m^2)	5.79	5.79	5.79
	Estimated maximum ε (trailing vortex) (W/kg)	***18.80***	***18.80***	***18.80***
	Vessel averaged turbulent shear rate (1/s)	827	827	827
	Impeller averaged turbulent shear rate (1/s)	***2276***	***2276***	***2276***
	Impeller averaged laminar shear rate (1/s)	110	110	110
	Particle settling velocity (cm/s)	0.18	1.93	4.23
Performance at N_{JS}	**Just suspended speed, N_{JS} (rpm)**	**609**	**930**	**1069**
	Total power input, P_{JS} (W)	0.08	0.29	0.44
	Power input per unit mass, ε_{JS} (W/kg)	0.281	1.004	1.522
	Reynolds number, Re_{JS} (-)	$3.15* 10^4$	$4.82* 10^4$	$5.53* 10^4$
	Tip speed, V_{tip_JS} (m/s)	1.12	1.70	1.96
	Bulk liquid velocity (m/s)	0.10	0.15	0.17
	Vessel averaged shear rate (1/s)	845	1596	1965
	Impeller averaged shear rate (1/s)	2327	4395	5411
	Impeller averaged laminar shear rate (1/s)	112	171	196

DSC Reports

DSC analysis were performed in a sealed gold-plated crucible, high pressure, 40 µL Mettler apparatus, under air, applying a heating rate of 5 °C/min in the range 0 °C to 400 °C.

The onset of decomposition of the starting material, the catalyst and the product are all below 150 °C, thus the thermal risk involved in storage and handling of these compounds can be considered low.

Thermogram Comparison between the Initial Reaction Mixture and Substrate *rac*-1

Pure *rac*-**1** (red)
Sample mass: 7.0000 mg.
The Substrate melts above 85 °C (MP = 101°C), then starts to decompose at 150 °C with a significant exothermic peak (159 J/g). A second decomposition phenomenon is observed at 215 °C.

Initial mixture, sampled immediately after CsF addition (black):
Sample mass: 12.9000 mg.
The initial mixture does not present any thermal instability close to the temperature of the process (22 °C). A weakly exothermic peak (40 J/g) is observed starting from 170 ° C, followed by further two slightly exothermic phenomena at 270 °C and 320 °C. Overall the mixture presents a similar profile to the starting material, with the exothermicity of the decomposition diminished due to the dilution in 1.4 vol of CH_2Cl_2.

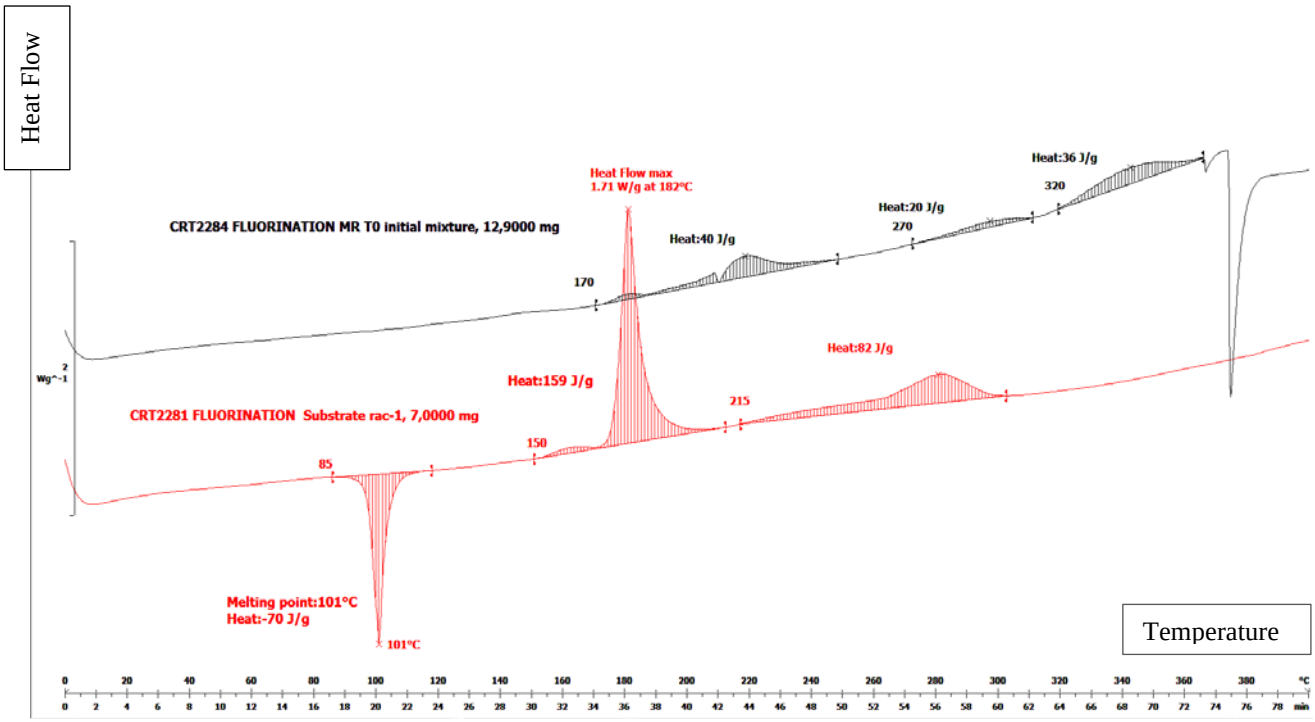

Figure S5: DSC curves of *rac*-**1** and initial reaction mixture.

Thermogram Comparison between the Final Reaction Mixture and Product (*R*,*R*)-2

Pure (*R*,*R*)-**2** (red):
Sample mass: 4.7500 mg.
The expected fluorinated product melts above 55 °C (MP = 77 °C). A small exothermic peak is visible in correspondence of the endothermic peak of melting and it is probably due to air oxidation. Starting from 215 °C, an exothermic decomposition of significant energy (274 J/g) is spread over a wide temperature range (ΔT= 160 °C) and it is characterized by a very slow onset of decomposition.

Final mixture, sampled after 48 h from CsF addition (black):
Sample mass: 11.3000 mg.
The final mixture shows the endothermic melting peak combined with solubilization starting from 85 °C. This is followed by specific heat change and two moderate exothermic phenomena at 245 °C (41 J/g) and 315 °C (74J/g) due to sample decomposition. The dilution effect of CH_2Cl_2 is noticeable.

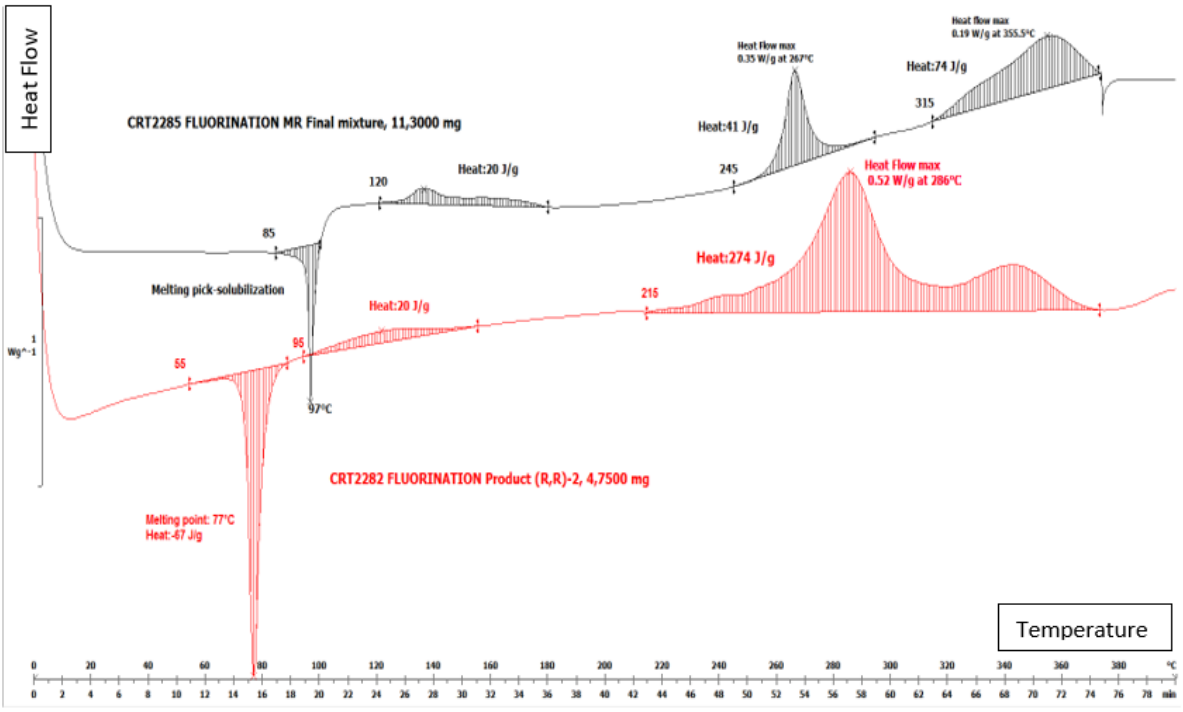

Figure S6: DSC curves of (*R*,*R*)-**2** and final reaction mixture.

Thermogram of Catalyst (*S*)-3

Sample mass: 4.6000 mg.

The catalyst (*S*)-**3** melts from 210 °C (MP = 228 °C) immediately followed by an exothermic peak of moderate energy (64.5 J/g) overlapped to the melting endotherm. An endothermal decomposition follows from 275 °C probably due to gas release.

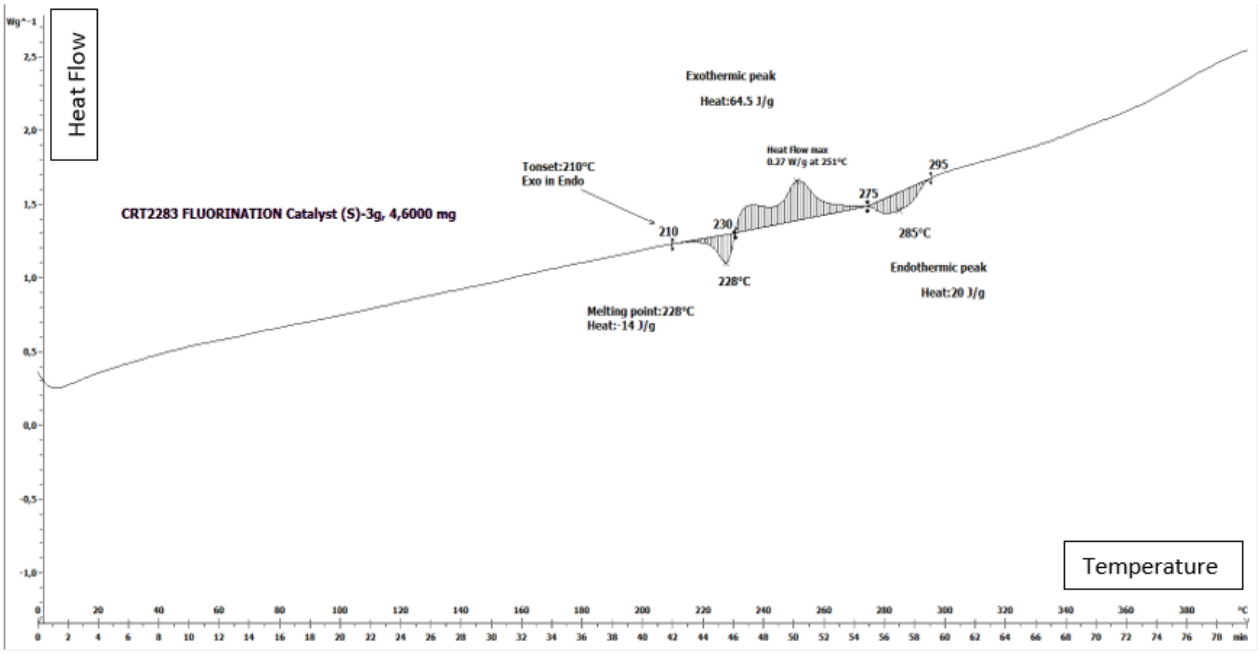

Figure S7: DSC curves of catalyst (*S*)-**3**.

Reaction Calorimetry

The fluorination on 200 g of *rac*-**1** was performed in a Mettler Toledo OptiMax (HTCal = heat flow calorimeter). The set-up and charging protocol are reported in the experimental section of the manuscript (section 4.2). An initial calibration was performed on the solution of *rac*-**1** (200 g, 0.558 mol) in CH_2Cl_2 (250 mL), before addition of catalyst (*S*)-**3** and CsF. A second calibration was performed after 48 h from the addition of CsF, when the reaction was almost complete (97% ^{19}F NMR yield of (*R*,*R*)-**2**). The initial and final heat exchange coefficient (U) and specific heat (C_p) of the reaction mass obtained in the calibration are reported in table S4.

Table S4: Calibration Data

Calibration	UA (W/K)	U (W/(K*m^2))	C_p (J/(g*K))
Initial	3.51	102	1.12
Final	3.49	98.6	0.95

The graph of the heat flow as function of time (orange) is shown in Figure S8, alongside the temperature of the reaction mass (red). The heat flow measured immediately after addition of CsF reached its maximum value and then it declined steadily. Samples for reaction monitoring via ^{19}F NMR were taken after 3.5 h, 22 h, 29 h and 46 h. These perturbations are clearly visible in Figure S8. From integration of the heat flow as function of time ($q_{r(t)}$) an energy release of 16.8 kJ was calculated (table S6). The signal is weak and recorded over a long period of time (48 h), which prevents an accurate measurement of the heat generated by the fluorination. This in turn affects the accuracy in the determination of ΔT_{ad}. From q_r a reaction enthalpy of –30 kJ/mol of *rac*-**1** (or an energy release of 34.7 kJ/kg reaction mass) has been calculated. The temperature increase of the reaction mass in adiabatic conditions is estimated to be 28 °C.

Figure S8: Thermogram for the enantioselective fluorination of 200 g of *rac*-**1** with CsF under HB-PTC. Red: Temperature inside the reactor; orange: heat flow due to the reaction.

Table S5: Thermochemical data

	Value	Comment
q_r	+16.8 kJ	Calculated by integration of the heat flow (q_r) as function of time using the Mettler Toledo Software A positive value is associated to an exothermic event.
rac-**1**	0.558 mol	MW *rac*-**1** = 358.32 g/mol
$\Delta H_{reaction}$/*rac*-**1**	–30 kJ/mol	= Q_r/(mol *rac*-**1**) ΔH is negative for an exothermic reaction.
ΔT_{ad}	28 °C	= Qr/(Cp*m) where m is the whole reaction mass

Catalyst Recovery

Recovery of (*S*)-**3** can be done either by silica-gel flash column chromatography (heptane, $^{i}Pr_2O$= 100% to 80:20, gradient; 46−67%) or by recrystallization (heptane 5mL/g and EtOH 1 mL/g; 52%). The first method was employed to recover the catalyst from the small-scale (1−50 g) screening reactions reported in the main text (Table 3, entries 4−7) and furnished (*S*)-**3** used in the fluorination described in entry 3 of Table S6; (*S*)-**3** recovered by crystallization from the 200 g scale was used for the experiment reported in entry 4 (Table S6). In both cases, the reactivity and selectivity obtained for the fluorination carried out with recycled catalyst (*S*)-**3** were unaltered (entries 1−4). The catalyst from these experiments was recycled a second time with no loss of reactivity and selectivity (entry 5).

Table S6: Fluorination with Recovered Catalyst

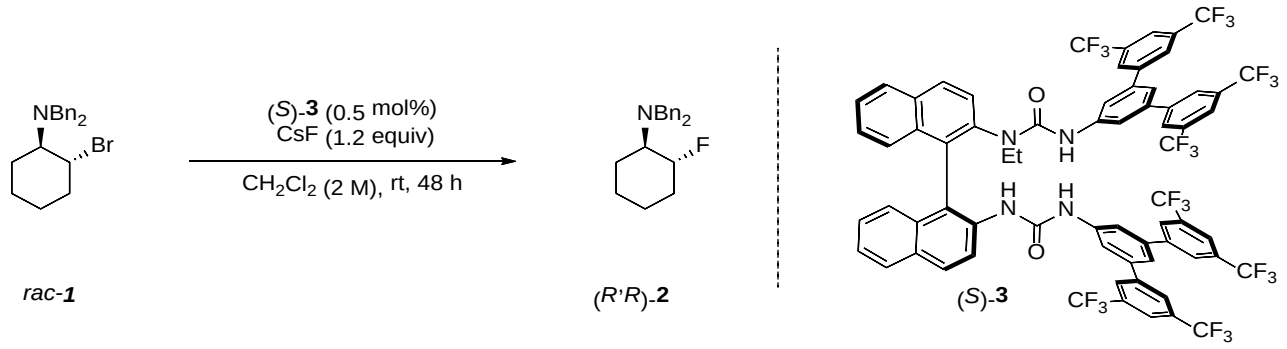

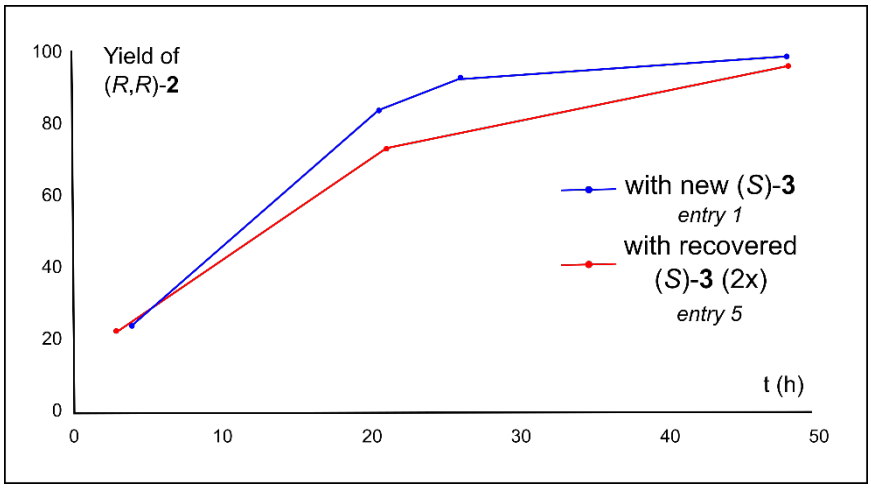

Entry	*Rac*-1	Cycle	Yield[b]	e.r.[c]	(*S*)-3 Recovery[d]
1	10 g	0	93%	82:18	46%
2	5 g	0	91%	81:19	65%
3[e]	5 g	1	89%	81:19	67%
4[f]	5 g	1	88%	82:18	59%
5[g]	4.5 g	2	81%	81.5:18.5	–

Conditions: *rac*-**1**, CsF (1.2 equiv), (*S*)-**3** (0.5 mol%), CH_2Cl_2 (2 M), rt, stirring at 900 rpm for 48 h. [a] Yield determined by ^{19}F NMR using 4-fluoroanisole as internal standard. [b] Yield of isolated (*R*,*R*)-**2**. [c] e.r. determined by HPLC on a chiral non-racemic stationary phase. [d] The catalyst was recovered by silica-gel flash column chromatography (FCC) using a CombiFlash. [e] (*S*)-**3** used in the fluorination was recovered by FCC with a CombiFlash from the reaction on 50 g of *rac*-**1**. [f] (*S*)-**3** used in the fluorination was recovered by recrystallization from the reaction on 200 g of *rac*-**1**. [g] (*S*)-**3** used in the fluorination was recovered by FCC with a CombiFlash from entries 3 and 4.

Catalyst's Side-Reactions

Full recovery of catalyst (*S*)-**3** was not possible due to its participation in side-reactions (Figure S9). Purification of recovered catalyst by silica-gel flash column chromatography allowed to isolate compound **4** (Figures S10 and S11) as the main side-product, alongside a complex mixture containing fluorinated products (signals at -62.4 – -62.7 ppm in the ^{19}F NMR spectrum). The identity of these products was not determined.

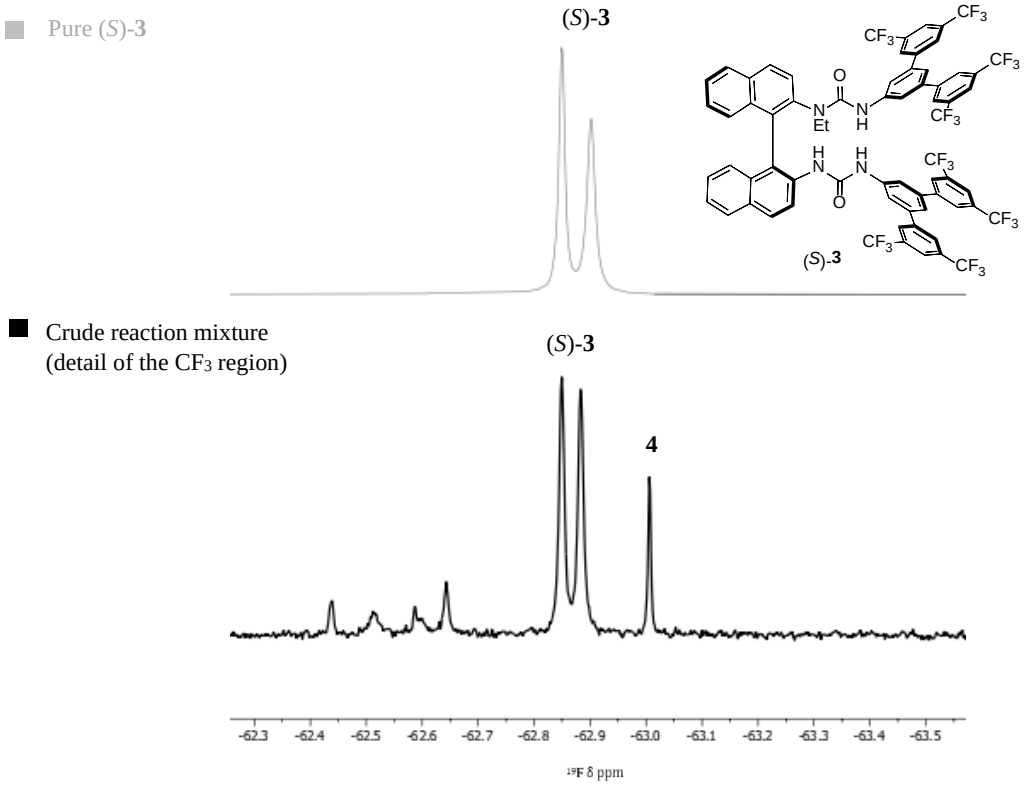

Figure S9: Detail of the CF_3 region of the ^{19}F NMR of catalyst (*S*)-**3 (**top, gray) and of the crude reaction mixture of the fluorination of *rac*-**1** with CsF using 1 mol% of (*S*)-**3** (bottom, black).

No degradation was observed when stirring (*S*)-**3** with *rac*-**1** in absence of CsF, while the extent of degradation appears to be dependent on catalyst loading, but not on CsF batch (Table S7, entries 2–7). Moreover, if KF is used as fluorine source, the catalyst is recovered intact (entry 1).

Table S7: Catalyst Degradation[a]

Entry	(*S*)-**3** loading (mol%)	MF	Recovery of (*S*)-**3**[a]	Yield of **4**[a]
1[b]	5	KF	93%	–
2	5	CsF 99.9%	81%	traces
3	5	CsF 99%	77%	traces
4	5	CsF 99% dry[c]	83%	traces
5	0.5	CsF 99.9%	31%	16%
6	0.5	CsF 99%	40%	16%
7	0.5	CsF 99% dry[c]	35%	19%

Conditions: *rac*-**1** (180 mg, 0.5 mmol), CsF (91.6 mg, 1.2 equiv), (*S*)-**3** (0.5–5 mol%), CH_2Cl_2 (500 µL, 1 M), rt, stirring at 900 rpm for 24 h. The main product obtained is β-fluoroamine (*R*,*R*)-**2**. [a] Determined by ^{19}F NMR using 4-fluoroanisole as internal standard. [b] 72 h, 5 equiv of KF. [c] Dried *in vacuo* at 200 °C for 48 h. The reaction was performed using Schlenk technique.

Assignment of 4

Assignment of **4** was based on NMR and HRMS analysis. ^{1}H NMR, ^{13}C NMR and HRMS were compatible with the reaction of nucleophilic substitution of (*S*)-**3** on *rac*-**1**. Key correlations in the ^{1}H–^{13}C HMBC spectrum reveal that the reaction took place on the unsubstituted urea (Figure S10). A further correlation between NH_B and the carbon in the ortho position of the terphenyl ring was visible, excluding alkylation of the external nitrogen (Figure S11). The information collected were not sufficient to discriminate between *N*- (**4a**) or *O*-alkylation (**4b**). The urea can attack either carbon of the aziridinium ion, giving rise to two diastereoisomers: (*S*,*R*,*R*) or (*S*,*S*,*S*), where the first term refers to the chiral axis of the BINAM scaffold of the catalyst and the second and third term arise from desymmetrisation of the aziridinium ion. **4** was isolated as a single diastereoisomer. Attempts to grow crystals of **4** suitable for X-ray analysis to confirm its structure (*N*- or *O*-alkylation) and determine its absolute configuration were unsuccessful. We were unable to isolate the other diastereoisomer and determine a diastereomeric ratio, but we cannot exclude its formation, as we did not fully characterise all the degradation products of the catalyst due to the difficulties in separating them. A similar degradation pathway was observed for thiourea organocatalysts and episulfonium ions.[1]

Detail of the ^{1}H-^{13}C HMBC of 4

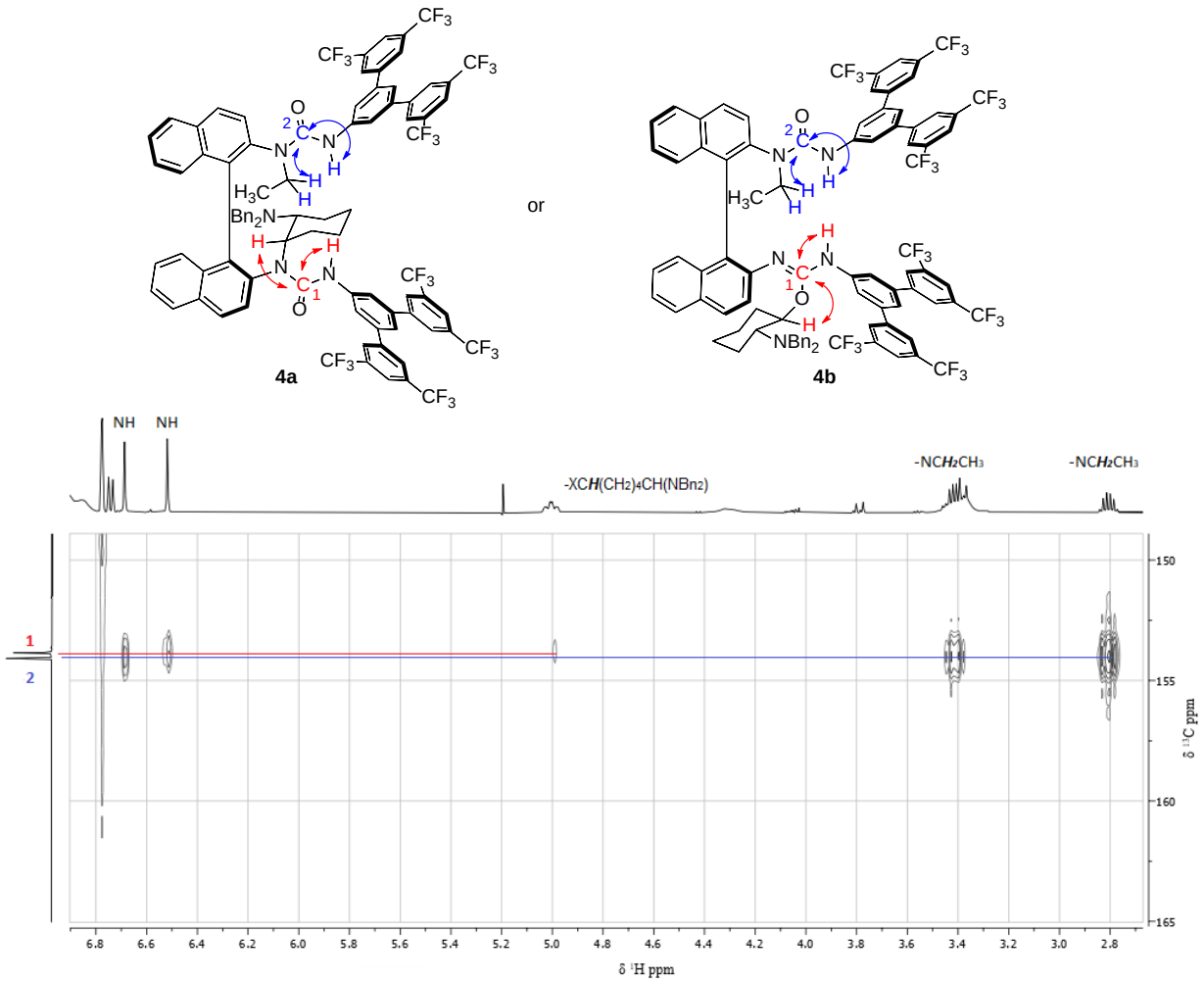

Figure S10: Detail of the ^{1}H-^{13}C HMBC showing correlation of the two C=O with two different NH and with the methylene of the ethyl chain and the methine of the cyclohexyl respectively. X=N or O.

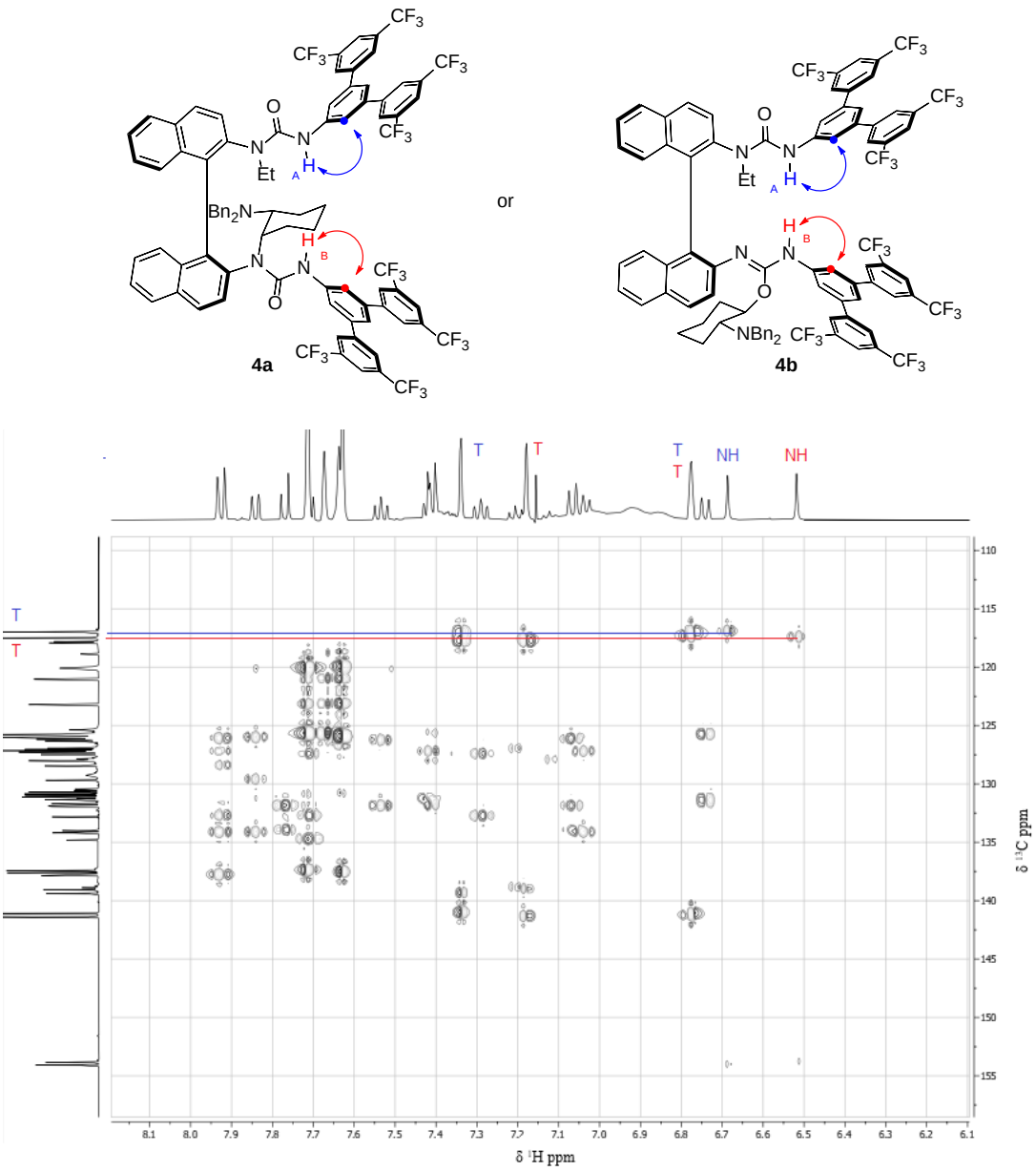

Figure S11: Detail of the ^{1}H-^{13}C HMBC showing correlation between the NH protons and the carbons of the terphenyl system in the ortho position. T= terphenyl.

Characterization of 4

White solid. **^{1}H NMR** (500 MHz, $CDCl_3$) δ 7.95 – 7.90 (m, 2H, overlapped signals), 7.84 (d, *J* =8.4 Hz, 1H), 7.77 (d, *J* = 8.8 Hz, 1H), 7.73–7.69 (m, 5H), 7.67 (s, 2H), 7.65 –7.62 (m, 6H), 7.53 (t, *J* = 7.5 Hz, 1H), 7.46 – 7.33 (m, 5H), 7.29 (t, *J* = 8.2, 1H), 7.23 – 7.16 (m, 3H), 7.15 – 6.80 (m, 10H), 6.79– 6.77 (m, 2H), 6.74 (d, *J* = 8.6 Hz, 1H), 6.69 (s, 1H, N**H**), 6.52 (s, 1H, N**H**), 5.00 (td, *J* = 11.6, 4.3 Hz, 1H), 4.31 (br s, 1H), 3.48– 3.30 (m, 4H), 2.81 (dq, *J* = 13.7, 6.8 Hz, 1H), 2.63 (td, *J* = 11.0, 3.5 Hz, 1H), 1.77– 1.69 (m, 1H), 1.27 – 1.16 (m, 1H), 1.08 – 0.99 (m, 2H), 0.86 – 0.77 (m, 2H), 0.64 (t, *J* = 6.9 Hz, 3H), -0.03 – -0.23 (m, 2H); **^{19}F NMR** (376 MHz, $CDCl_3$) [overlapping signals] δ –63.11; **^{13}C NMR** (126 MHz, $CDCl_3$) [overlapping signals] δ 155.3, 155.0, 142.6, 142.3, 140.6, 140.2, 139.0, 138.8, 138.6, 134.0, 135.4, 135.2, 134.0, 133.1, 133.0, 132.9, 132.5, 132.6, 132.2 (q, *J* = 33.3 Hz), 132.0 (q, *J* = 33.3 Hz), 130.9, 130.4 (br), 129.6, 129.2, 129.1 (br), 128.7, 128.5, 128.4, 128.2, 128.1, 127.6, 127.4, 127.4, 127.3, 127.2, 127.0, 126.9, 123.3 (q, *J* = 272.9 Hz), 123.4 (q, *J* = 273.0 Hz), 121.4–121.1 (m, 2 signals), 119.1, 119.0, 118.7, 118.2, 58.6, 57.9, 55.2 (br, Ph**C**H_2), 52.4 (br, Ph**C**H_2), 44.8 (**C**H_2CH_3), 33.2, 25.2, 24.2, 24.1, 12.7 (CH_2**C**H_3); **HRMS** (ESI$^+$) *m/z* calculated for $C_{88}H_{62}O_2N_5F_{24}$ $[M+H]^+$ 1676.4515, found 1676.4432.

NMR Spectra

(1*R*,2*R*)-*N*,*N*-dibenzyl-2-fluorocyclohexan-1-amine (After Aqueous Work-up)

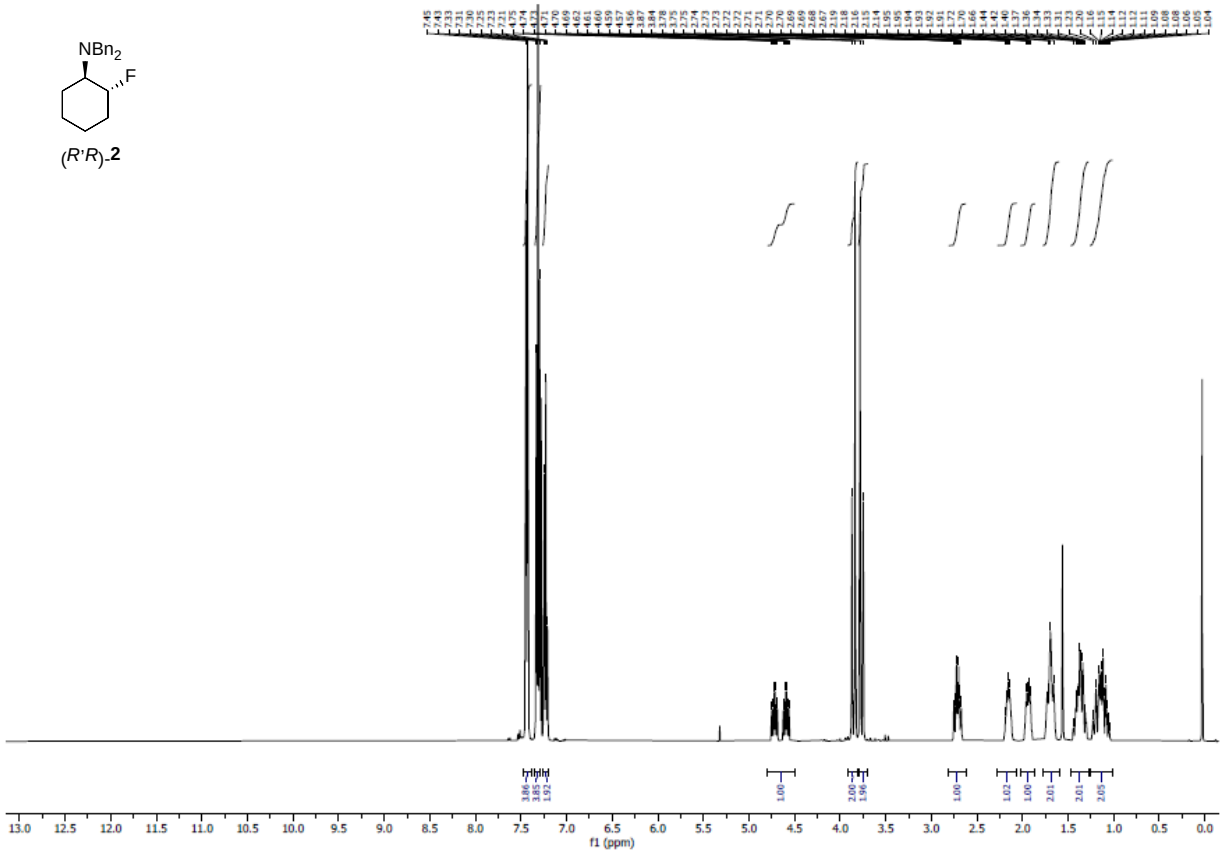

The NMR spectra were in agreement with those previously reported.[2]

(1*R*,2*R*)-*N*,*N*-dibenzyl-2-fluorocyclohexan-1-aminium 2,2,2-trifluoroacetate CF_3COOH*(*R*,*R*)-2 (After Recrystallization)

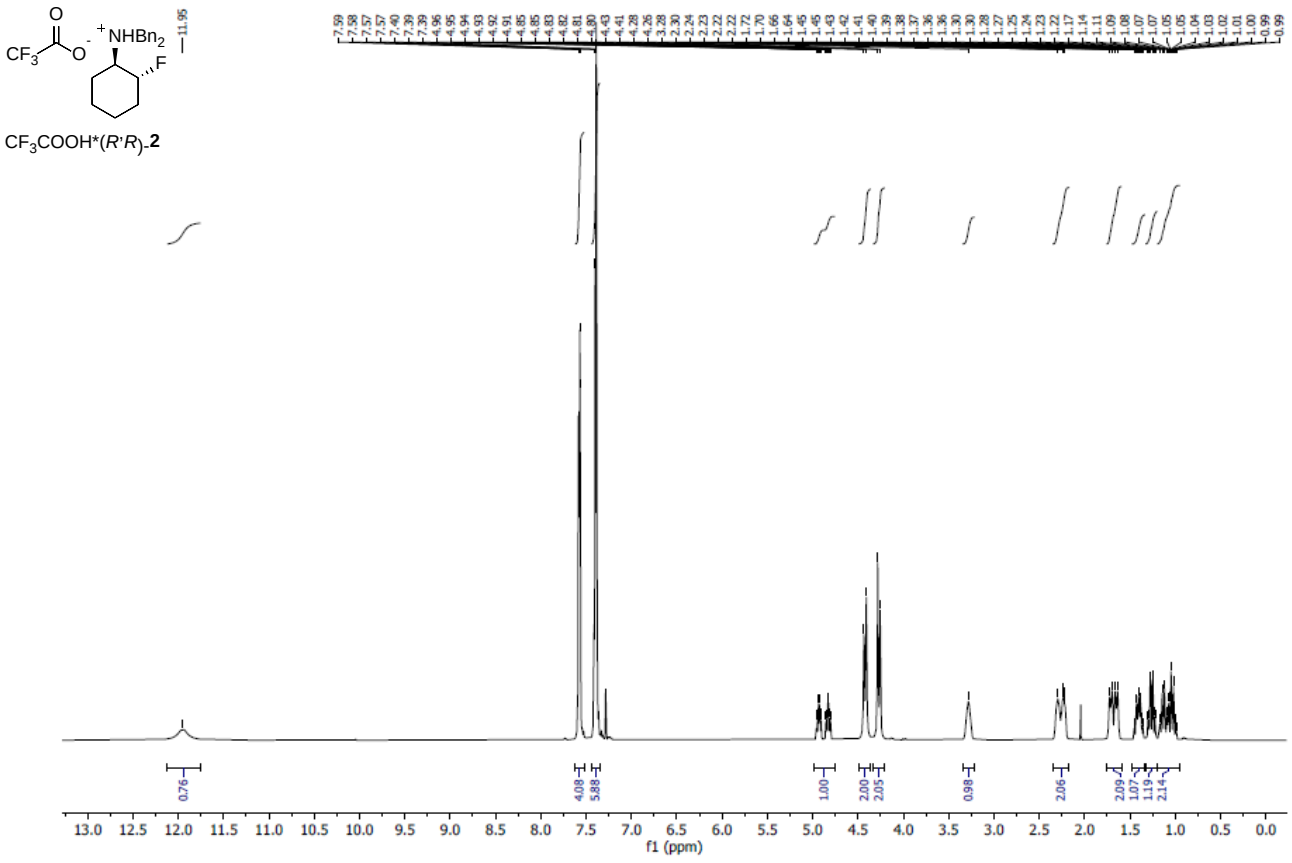

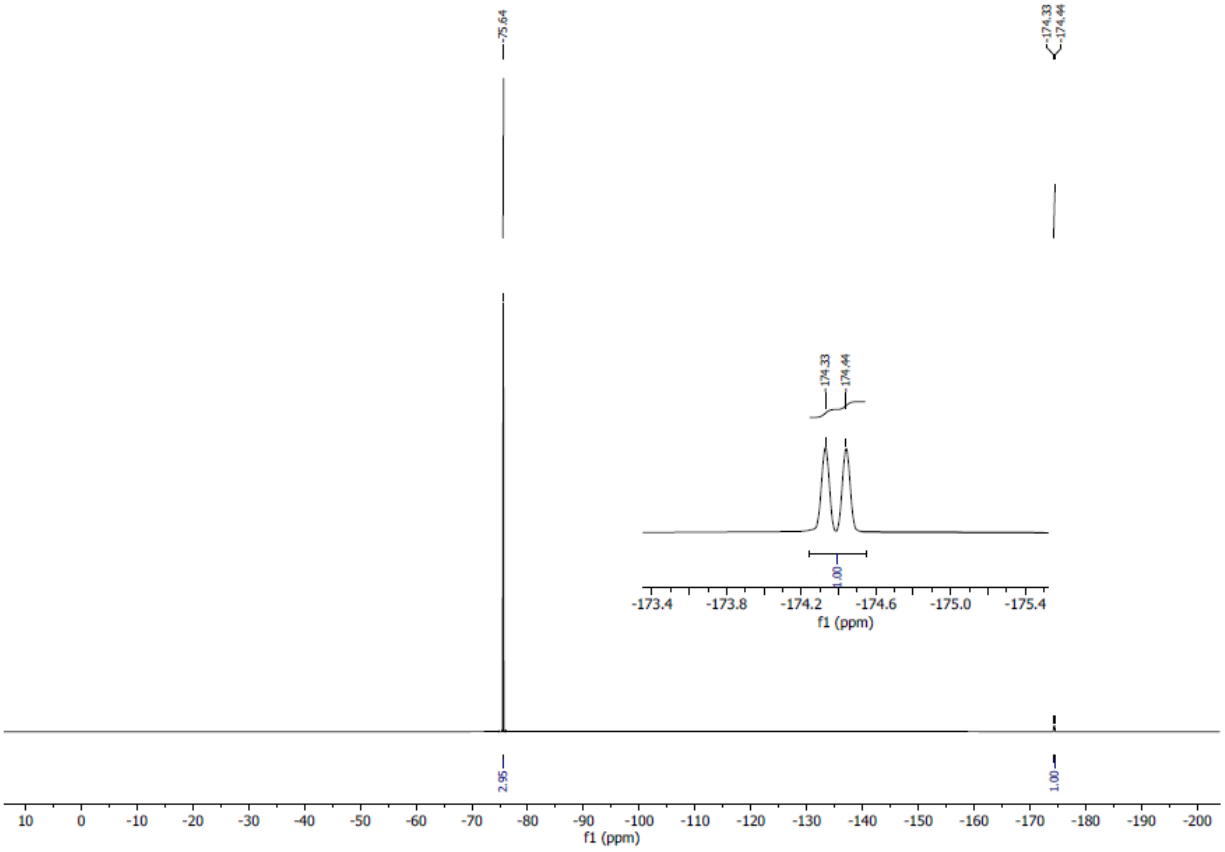

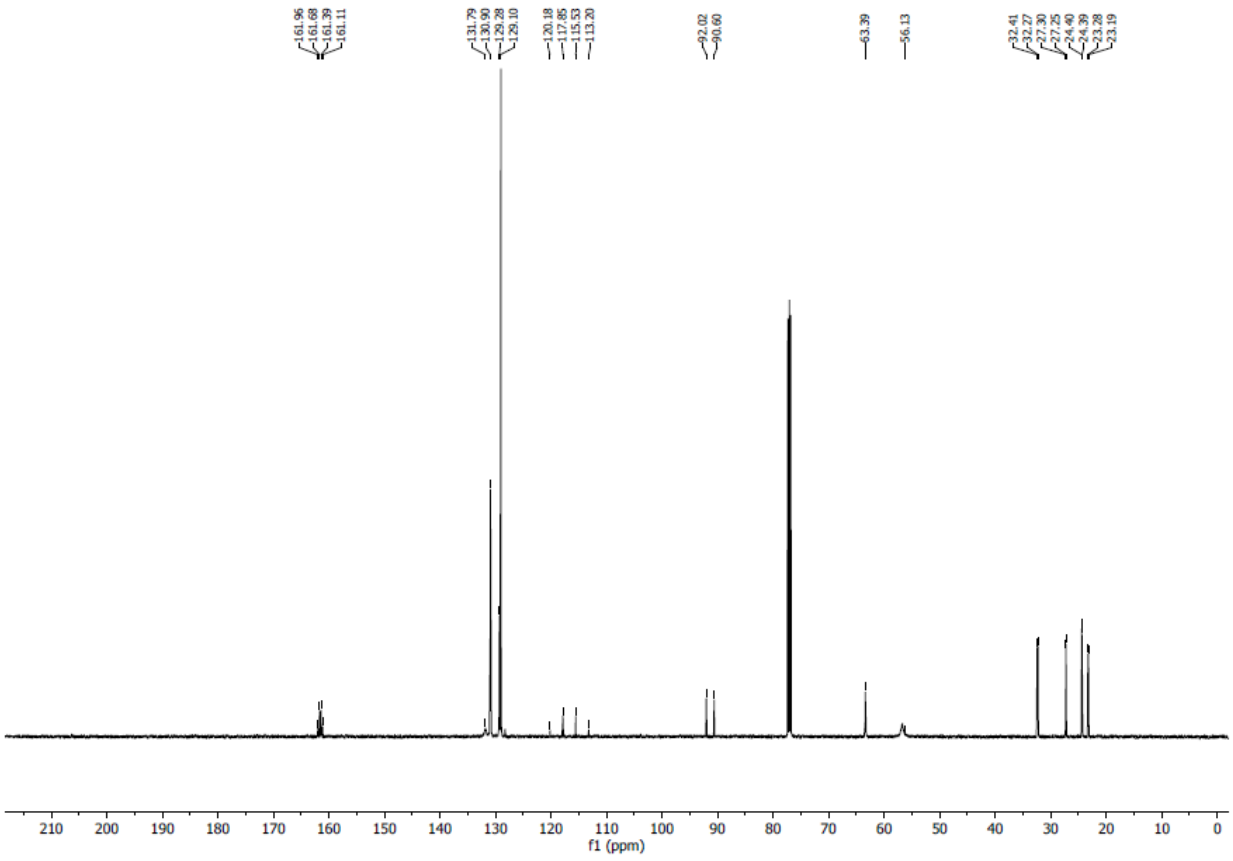
161.96
161.68
161.39
161.11
131.79
130.90
129.28
129.10
120.18
117.85
115.53
113.20
92.02
90.60
63.39
56.13
32.41
32.27
27.30
27.25
24.40
24.39
23.28
23.19
210 200 190 180 170 160 150 140 130 120 110 100 90 80 70 60 50 40 30 20 10 0
f1 (ppm)

HPLC Traces

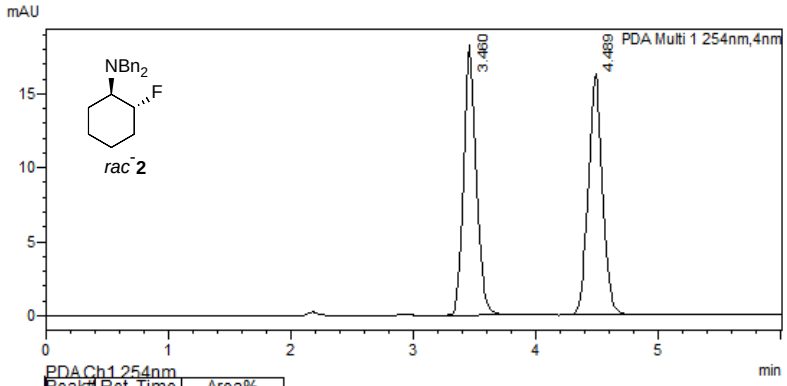

PDA Ch1 254nm

Peak#	Ret. Time	Area%
1	3.460	49.943
2	4.489	50.057

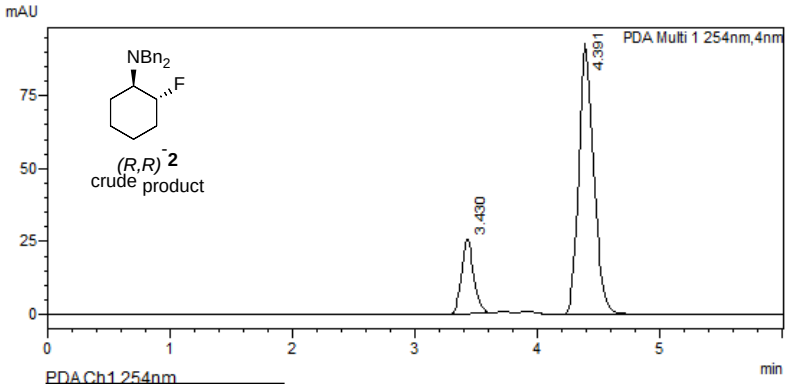

PDA Ch1 254nm

Peak#	Ret. Time	Area%
1	3.430	17.948
2	4.391	82.052

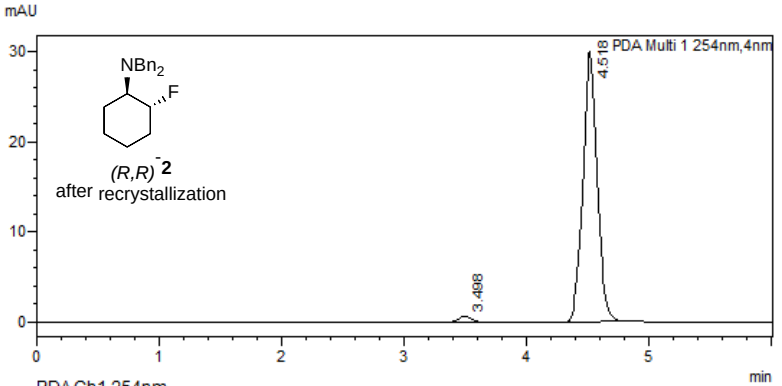

PDA Ch1 254nm

Peak#	Ret. Time	Area%
1	3.498	1.863
2	4.518	98.137

[1] Pupo, G.; Ibba, F.; Ascough, D. M. H.; Vicini, A. C.; Ricci, P.; Christensen, K. E.; Pfeifer, L.; Morphy, J. R.; Brown, J. M.; Paton, R. S.; Gouverneur, V. Asymmetric Nucleophilic Fluorination under Hydrogen Bonding Phase-Transfer Catalysis *Science*, **2018**, *360*, 638–642.

[2] Pupo, G.; Vicini, A. C.; Ascough, D. M. H.; Ibba, F.; Christensen, K. E.; Thompson, A. L.; Brown, J. M.; Paton, R. S.; Gouverneur, V. "Hydrogen Bonding Phase-Transfer Catalysis with Potassium Fluoride: Enantioselective Synthesis of β-Fluoroamines" *J. Am. Chem. Soc.*, **2019**, *141*, 2878.